Supporting Information

Interaction potential energy surface between superatoms

Qingyue Zhang[a∇], *Yang Gao*[a,b∇], *Rui Wang*[a], *Yu Zhu*[a], *Weiyu Xie*[a], *Georg Schreckenbach*[b*] *and Zhigang Wang*[a,c*]

[a] Institute of Atomic and Molecular Physics, Jilin University, Changchun 130012, China
[b] Department of Chemistry, University of Manitoba, Winnipeg, Manitoba, R3T 2N2, Canada
[c] Institute of Theoretical Chemistry, Jilin University, Changchun 130023, China
[∇] these authors contributed equally to this work.
*To whom correspondence should be addressed. E-mail: wangzg@jlu.edu.cn (Z. W.), schrecke@cc.umanitoba.ca (G. S.)

Contents

Part 1. Computational details

In this study, we selected the $(Pa@C_{28})_2$ dimer for superatom rigid potential energy surface scans. Considering the large size of the system and the need to study different electronic states, density functional theory (DFT)[1, 2] and the corresponding time-dependent density functional theory (TD-DFT)[3] were applied. Previously, the M06-2X level has been shown to be appropriate for the calculation of inter-superatomic interactions[4, 5]. Various other functionals (LSDA, PBE, PW91, BP86, BLYP, B3LYP, PBE0, HSE06, M06-2X), when applied to the electronic structure of actinide embedded fullerene, have all reached consistent conclusions[6, 7]. Therefore, the hybrid meta generalized gradient approximation at the M06-2X level with dispersion was adopted for this study. In terms of (scalar) relativistic effects, a small-core relativistic effective core potential (RECP) covering 60 core electrons with a corresponding (14s13p10d8f6g)/ [10s9p5d4f3g] valence basis set[8] was used for Pa, while C was modeled with the valence double-ζ with d-polarization basis set 6-31G*[9]. Meanwhile, we also used the 6-311G* basis set for C for methodological comparison. These calculations were carried out using the Gaussian16 A.03 program[10].

Table S1. Coordinates of the optimized structure $(Pa@C_{28})_2$.

Number	Atom	x(Å)	y(Å)	z(Å)
1	Pa	3.519400	-0.003205	0.006453
2	C	5.597924	0.729903	-1.169167
3	C	3.493245	-2.486941	0.213833
4	C	3.404016	1.050712	2.262286
5	C	1.457366	0.731420	-1.350854
6	C	2.668408	-1.172174	1.988261

7	C	3.547707	1.808529	-1.634911
8	C	3.579937	0.520579	-2.380791
9	C	4.164609	-1.163896	2.039204
10	C	1.412960	0.830666	1.027090
11	C	4.836716	-1.473204	-1.427426
12	C	5.533103	-1.355252	-0.104599
13	C	2.194867	1.995042	0.505087
14	C	1.469054	-1.381792	-0.253451
15	C	5.477735	0.841324	1.167247
16	C	4.748927	2.020244	0.595486
17	C	2.282008	-1.478288	-1.506004
18	C	0.764924	0.018457	-0.151258
19	C	3.433273	2.097855	1.258609
20	C	3.539746	-2.136275	-1.193230
21	C	5.989083	0.034199	0.049496
22	C	2.265854	-1.941193	0.803265
23	C	2.301264	-0.151487	-2.122161
24	C	4.605905	0.230262	2.170635
25	C	4.787567	1.900687	-0.851077
26	C	2.211113	0.222006	2.055679
27	C	4.661096	-1.954266	0.905748
28	C	2.250612	1.870481	-0.951452
29	C	4.839239	-0.158391	-2.043418
30	Pa	-3.519400	0.003205	0.006453
31	C	-5.597924	-0.729902	-1.169168
32	C	-3.404016	-1.050713	2.262286
33	C	-1.457366	-0.731418	-1.350855
34	C	-3.493245	2.486941	0.213836
35	C	-1.412960	-0.830667	1.027089
36	C	-4.836716	1.473205	-1.427425
37	C	-5.533103	1.355252	-0.104598
38	C	-2.194867	-1.995043	0.505085
39	C	-1.469055	1.381792	-0.253449
40	C	-5.477735	-0.841325	1.167246
41	C	-4.748927	-2.020245	0.595484
42	C	-2.282008	1.478289	-1.506003
43	C	-2.668408	1.172173	1.988262
44	C	-3.547707	-1.808527	-1.634913
45	C	-3.579937	-0.520577	-2.380791
46	C	-4.164609	1.163895	2.039205
47	C	-2.265855	1.941193	0.803266
48	C	-2.301264	0.151489	-2.122161
49	C	-4.605905	-0.230264	2.170635
50	C	-4.787567	-1.900686	-0.851079

51	C	-2.211113	-0.222008	2.055679
52	C	-4.661097	1.954265	0.905750
53	C	-2.250612	-1.870480	-0.951453
54	C	-4.839239	0.158393	-2.043418
55	C	-0.764924	-0.018457	-0.151258
56	C	-3.433273	-2.097856	1.258607
57	C	-3.539746	2.136276	-1.193229
58	C	-5.989083	-0.034199	0.049496

Table S2. Potential energy changes of singlet state S_0-S_3 and triplet state T_1-T_3 with distance, with C atom basis sets 6-31G* and 6-311G* (in brackets).

ΔE(eV)	**S_0**	**S_1**	**S_2**	**S_3**	**T_1**	**T_2**	**T_3**
6.73 Å	2.1749	4.6476	4.6605	5.3840	4.4434	4.4540	4.8330
	(2.1376)	(4.6156)	(4.6319)	(5.3463)	(4.4113)	(4.4245)	(4.7883)
7.03 Å	0.0000	2.4489	2.4581	3.2056	2.2524	2.2609	2.6486
	(0.0000)	(2.4542)	(2.4672)	(3.2051)	(2.2571)	(2.2689)	(2.6416)
7.53 Å	1.3939	3.4139	3.4183	4.0270	3.2812	3.2854	3.4331
	(1.3878)	(3.4099)	(3.4201)	(4.0087)	(3.2773)	(3.2865)	(3.42131)
8.23 Å	3.2034	4.5260	4.5284	5.0241	2.3320	4.4358	4.4381
	(3.1865)	(4.5103)	(4.5110)	(4.9849)	(2.3391)	(4.4207)	(4.42139)

Part 2. Mayer bond order analysis of the C-C bond from 1.53 Å to 2.53 Å.

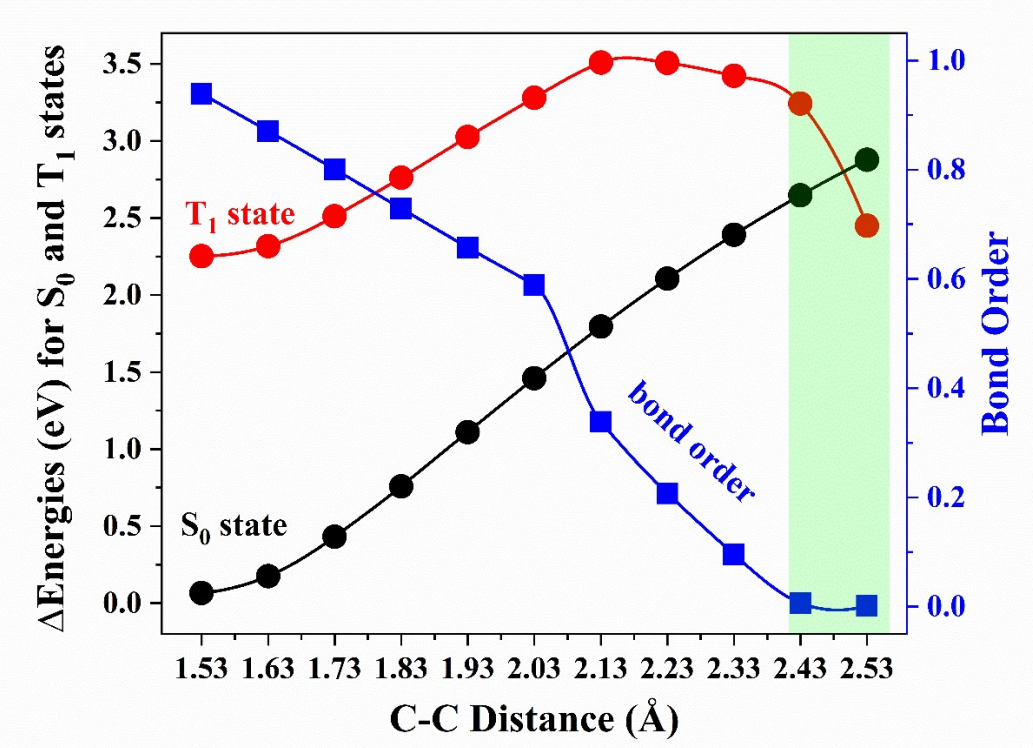

Figure S1. Mayer bond order analysis of the C-C bond from 1.53 Å to 2.53 Å. The blue line represents the change of bond order with the C-C distance. The black and red lines represent the energies of the S_0 and S_1 states as a function of the C-C distance, respectively.

Part 3. Symmetry of the system.

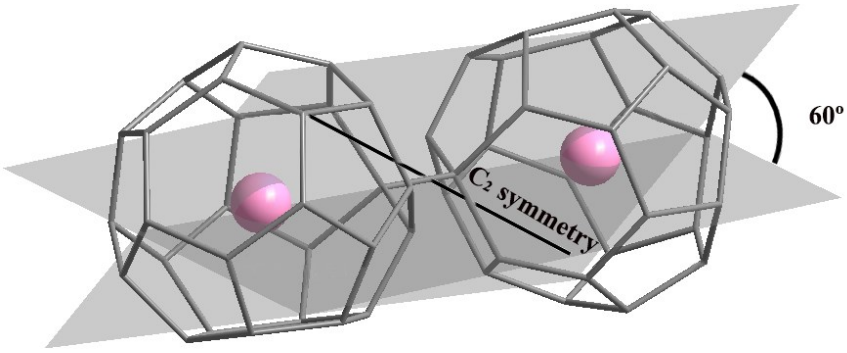

Figure S2. The solid black line is the C_2 symmetry axis of the system. The two planes are the respective symmetry planes of the two monomers, and the angle between them is 60^{o}.

Part 4. Details for energy decomposition analysis (EDA).

To understand inter-superatomic interactions, energy decomposition analysis (EDA)[11] was performed with the ADF 2012 package[12], using DFT with empirical dispersion corrections (DFT-D3)[13] at the Perdew-Burke-Ernzerhof (PBE) level[14]. PBE is a widely used functional in embedded systems of actinides[6, 7]. Scalar relativistic corrections have been taken into consideration by the zeroth order regular approximation (ZORA)[15]. Triple-ζ polarized (TZP) uncontracted Slater-type orbital basis sets have been used, with a [$1s^2$-$4f^{10}$] frozen core for Pa[16] and no frozen core (all- electron basis set) for C atoms.

In the EDA method, ΔE_{int} is the interaction energy between two fragments in specific electronic reference states. The interaction energy is then divided into four primary components:

$$\Delta E_{int} = \Delta E_{elstat} + \Delta E_{Pauli} + \Delta E_{orb} + \Delta E_{dis}$$

ΔE_{elstat} corresponds to the electrostatic interaction between the two fragments; ΔE_{Pauli} is a destabilizing interaction between occupied orbitals; and ΔE_{orb} is the result of the interactions between occupied orbitals of one fragment and the vacant orbitals of the other. Finally, ΔE_{dis} represents the dispersion correction energy.

Table S3. Absolute values of EDA with angle change for rotation around R axis.

R	**0°**	**30°**	**60°**	**90°**

E_{orb} **(eV)**	-15.63	-15.69	-15.77	-15.67
E_{elstat} **(eV)**	-7.64	-7.68	-7.72	-7.68
E_{dis} **(eV)**	-0.32	-0.31	-0.31	-0.31

Table S4. Absolute values of EDA with angle change for rotation around R_1-axis.

R_1	**0°**	**60°**	**120°**	**180°**	**240°**	**300°**
E_{orb} (eV)	-15.63	-5.27	-5.24	-6.60	-5.39	-5.41
E_{elstat} (eV)	-7.64	-3.06	-2.94	-3.41	-3.01	-3.16
E_{dis} (eV)	-0.32	-0.31	-0.30	-0.30	-0.31	-0.31

Table S5. Absolute values of EDA with angle change for rotation around R_2-axis.

R_2	**0°**	**60°**	**120°**	**180°**	**240°**	**300°**
E_{orb} (eV)	-15.63	-1.63	-1.44	-6.70	-3.12	-3.87
E_{elstat} (eV)	-7.64	-2.12	-1.87	-3.52	-2.37	-2.73
E_{dis} (eV)	-0.32	-0.51	-0.50	-0.49	-0.49	-0.50

Table S6. Absolute values of EDA with angle change for rotation around R_3-axis.

R_3	**0°**	**60°**	**120°**	**180°**	**240°**	**300°**
E_{orb} (eV)	-15.63	-3.77	-5.04	-6.73	-1.39	-1.57
E_{elstat} (eV)	-7.64	-3.16	-3.09	-3.49	-1.73	-1.84

E_{dis} (eV)	-0.32	-0.31	-0.30	-0.30	-0.30	-0.31

Part 5. Orbital analysis.

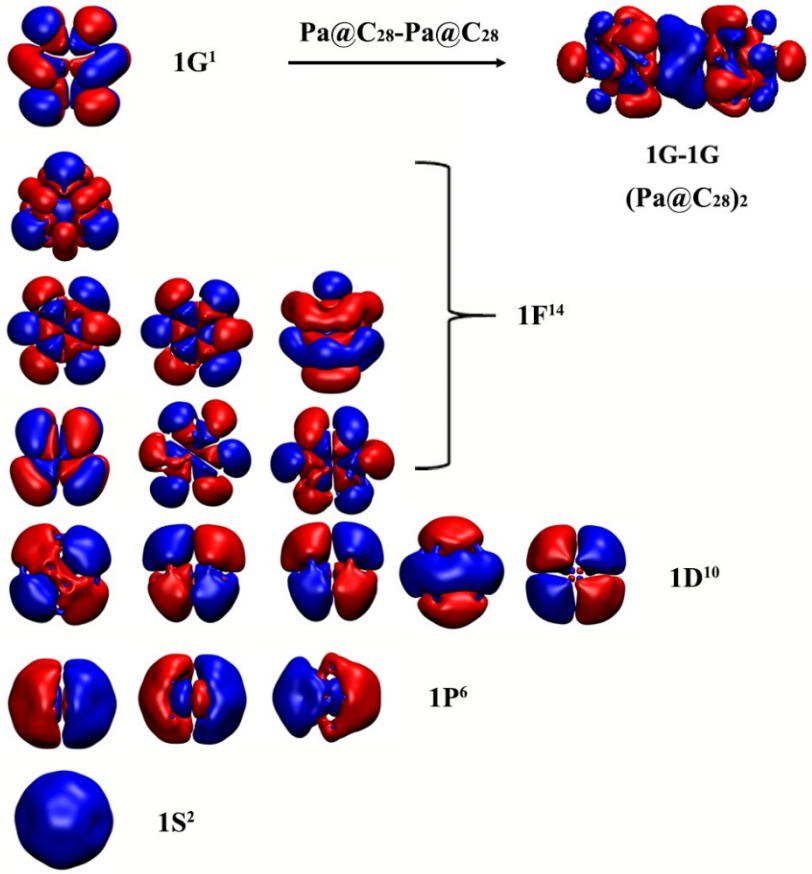

Figure S3. Valence electron orbitals of $Pa@C_{28}$ and the 1G-1G orbital formed by the interaction of two $Pa@C_{28}$.

Part 6. Selection of R_1-axis, R_2-axis and R_3-axis.

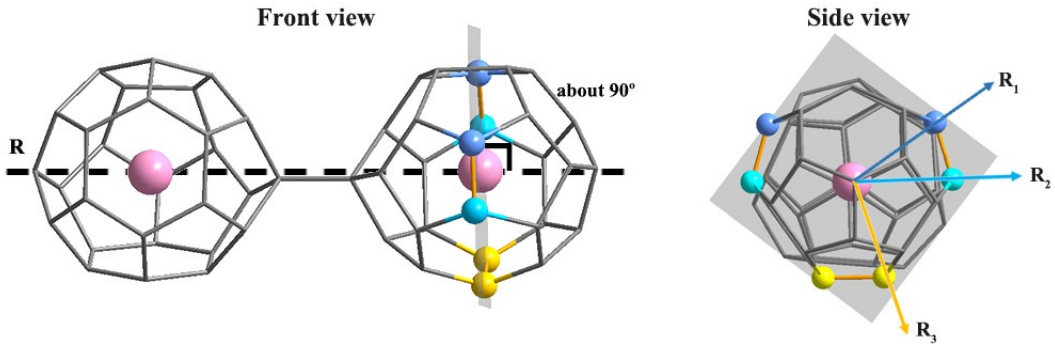

Figure S4. Schematic diagram of the three axes (R_1-axis, R_2-axis, and R_3-axis) perpendicular to the R-axis.

Since Pa@C_{28} is a sphere-like structure, we consider it approximately as a sphere. We set the single bond formed between two superatoms as the R axis. Then we choose three atoms on a Pa@C_{28} superatom, which are on a plane that passes through the Pa atom and perpendicular to the R axis, and are symmetric with the other three atoms on the plane. These three atoms are connected to the central atom Pa to form the R_1-axis, R_2-axis and R_3-axis.

Part 7. Change in bond length when rotated by 180º.

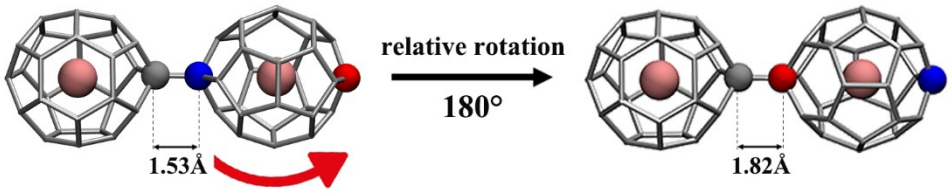

Figure S5. Cage deformation is seen around the C atoms in contact.

Part 8. Electron density difference analysis.

Considering the importance of charge transfer, quantitative analysis by electron density difference integrals was performed using Multiwfn 3.7[17]. For this purpose, we placed $(Pa@C_{28})_2$ in the spherical coordinate system and define the line between the superatoms as the x-axis. Then, the electron deformation density in the y and z directions is integrated onto the x-direction: $I(x) = \int_{-\infty}^{+\infty} \Delta\rho(x,y,z)dydz$, where $\Delta\rho$ is the electron density of the complex minus that of the two isolated fragments. The corresponding value of $I(x)$ measures the amount of electronic charge accumulation or depletion relative to the non-interacting fragments. The coordinate origin is the midpoint between the two isolated fragments.

References

1. L. Andrews, B. Liang, J. Li and B. E. Bursten, *J. Am. Chem. Soc.*, 2003, **125**, 3126-3139.
2. T. Guo, M. D. Diener, Y. Chai, M. J. Alford, R. E. Haufler, S. M. McClure, T. Ohno, J. H. Weaver, G. E. Scuseria and R. E. Smalley, *Science*, 1992, **257**, 1661.
3. P. Elliott, F. Furche and K. Burke, *Rev. Comput. Chem.*, 2007, **26**, 91-165.
4. Y. Zhao and D. G. Truhlar, *Theor. Chem. Acc.*, 2008, **120**, 215-241.
5. E. G. Hohenstein, S. T. Chill and C. D. Sherrill, *J. Chem. Theory Comput.*, 2008, **4**, 1996-2000.
6. X. Dai, Y. Gao, W. Jiang, Y. Lei and Z. Wang, *Phys. Chem. Chem. Phys,* 2015, **17**.
7. W. Xie, W. Jiang, Y. Gao, J. Wang and Z. Wang, *Chem. Commun.*, 2018, **54**, 13383-13386.
8. X. Cao and M. Dolg, *J. Mol. Struct.: THEOCHEM*, 2004, **673**, 203-209.
9. P. C. Hariharan and J. A. Pople, *Theor. Chim. Acta*, 1973, **28**, 213-222.
10. M. J. Frisch, G. W. Trucks, H. B. Schlegel, G. E. Scuseria, M. A. Robb, J. R. Cheeseman, G. Scalmani, V. Barone, G. A. Petersson, H. Nakatsuji, X. Li, M. Caricato, A. V. Marenich, J. Bloino, B. G. Janesko, R. Gomperts, B. Mennucci, H. P. Hratchian, J. V. Ortiz, A. F. Izmaylov, J. L. Sonnenberg, Williams, F. Ding, F. Lipparini, F. Egidi, J. Goings, B. Peng, A. Petrone, T. Henderson, D. Ranasinghe, V. G. Zakrzewski, J. Gao, N. Rega, G. Zheng, W. Liang, M. Hada, M. Ehara, K. Toyota, R. Fukuda, J. Hasegawa, M. Ishida, T. Nakajima, Y. Honda, O. Kitao, H. Nakai, T. Vreven, K. Throssell, J. A. Montgomery Jr., J. E. Peralta, F. Ogliaro, M. J. Bearpark, J. J. Heyd, E. N. Brothers, K. N. Kudin, V. N. Staroverov, T. A. Keith, R. Kobayashi, J. Normand, K. Raghavachari, A. P. Rendell, J. C. Burant, S. S. Iyengar, J. Tomasi, M. Cossi, J. M. Millam, M. Klene, C. Adamo, R. Cammi, J. W. Ochterski, R. L. Martin, K. Morokuma, O. Farkas, J. B. Foresman and D. J. Fox, *Journal*, 2016.
11. T. Ziegler and A. Rauk, *Theor. Chim. Acta*, 1977, **46**, 1-10.
12. G. te Velde, F. M. Bickelhaupt, E. J. Baerends, C. Fonseca Guerra, S. J. A. van Gisbergen, J. G. Snijders and T. Ziegler, *J. Comput. Chem.*, 2001, **22**, 931-967.
13. S. Grimme, J. Antony, S. Ehrlich and H. Krieg, *J. Chem. Phys.*, 2010, **132**, 154104.
14. J. Perdew, K. Burke and M. Ernzerhof, *Phys. Rev. Lett.*1996, **77**, 3865-3868.
15. E. v. Lenthe, E. J. Baerends and J. G. Snijders, *J. Chem. Phys.*, 1993, **99**, 4597-4610.
16. E. Van Lenthe and E. J. Baerends, *J. Comput. Chem.*, 2003, **24**, 1142-1156.
17. T. Lu and F. Chen, *J. Comput. Chem.*, 2012, **33**, 580-592.